processes

Article

Thermodynamic and Heat Transfer Performance of the Organic Triangle Cycle

Liang Liu [1,2], Siyuan Zhang [1,2], Youzhou Jiao [1,2], Xinxin Liu [1,2], Gang Li [1,2], Chao Liu [3], Qibin Li [3], Hao Guo [4] and Chao He [1,2,*]

1 Key Laboratory of New Materials and Facilities for Rural Renewable Energy of Ministry of Agriculture and Rural Affairs, College of Mechanical & Electrical Engineering, Henan Agricultural University, Zhengzhou 450002, China
2 Henan International Joint Laboratory of Biomass Energy and Nanomaterials, Henan Agricultural University, Zhengzhou 450002, China
3 Key Laboratory of Low-Grade Energy Utilization Technologies and Systems of Ministry of Education, College of Power Engineering, Chongqing University, Chongqing 400030, China
4 Key Laboratory of Cryogenics, Technical Institute of Physics and Chemistry, Chinese Academy of Sciences, Beijing 100190, China
* Correspondence: hechao666777@163.com

Abstract: Compared to the organic Rankine cycle (ORC), the organic triangle cycle (TC) is simpler in structure and is not limited by pinch point temperature differences. TC has been studied to some extent by previous researchers, such as the selection of working fluid, application, and the design of the expander. However, system optimization and parameter analysis of TC are still rare. The thermodynamic performance of TC internal circulation and TC heat recovery systems are investigated by theoretical analysis and numerical simulation, respectively. The results indicate that the expander inlet temperature T_3 and heater inlet temperature T_2 are key elements impacting the thermodynamic performance of the TC internal circulation. For the TC heat recovery system, an optimal value of the average heat-capacity flow rate of working fluid C_{wf} is discovered to output the maximum net power output W_{net}. Moreover, the total heat transfer coefficients for the heater $(kA)_h$ and condenser $(kA)_c$ are discussed in relation to C_{wf} variations. The findings will provide critical guidance for system investment and optimization.

Keywords: organic triangle cycle; thermodynamics analysis; low-grade energy

check for updates

Citation: Liu, L.; Zhang, S.; Jiao, Y.; Liu, X.; Li, G.; Liu, C.; Li, Q.; Guo, H.; He, C. Thermodynamic and Heat Transfer Performance of the Organic Triangle Cycle. *Processes* **2023**, *11*, 357. https://doi.org/10.3390/pr11020357

Academic Editors: Daria Bellotti, Giampaolo Manfrida, Xiaoyan Ji, Alessandro Sorce and Massimo Rivarolo

Received: 29 November 2022
Revised: 13 January 2023
Accepted: 20 January 2023
Published: 22 January 2023

1. Introduction

In today's world, the environment and development are both mutually constrained and interdependent. How to balance development and environment is a hot issue today. Researchers have studied the development and utilization of many clean, renewable energy sources, such as wind [1,2], solar [3,4], and geothermal [5,6] energy. Nowadays, geothermal water is mostly used for energy generation via direct heating, flash geothermal power generation, total flow geothermal power generation, binary cycle power generation, and total flow-binary cycle combined power generation [7,8]. Additionally, the organic triangle cycle (TC) [9] can be applied to recover geothermal energy, and it has gained much attention due to its advantages, such as its simple system and high exergy efficiency. Besides, TC is suitable for lower temperature heat sources compared to ORC, and TC has the potential to generate electricity even from heat sources below 80 °C in cases where ORC is not economically feasible [10,11]. As a result, several studies have been undertaken in this sector. Smith et al. [12–14] investigated the construction concept, use of mixed mixture working fluids, and two-phase expansion working principle of a Lysholm double screw expander, laying a solid platform for future TC research. Bryson [15] compared TC to the traditional double cycle and discovered that the TC had significant advantages when the expander adiabatic efficiency reached certain values. Steffen et al. [16] compared TC with ORC. The exergy efficiency of TC using water as working fluid was 35 to 70% higher than that of the supercritical ORC at heat source temperatures up to 450 K. Fischer et al. [17,18] compared the thermodynamic performances of single-stage TCs with water as the working fluid, the organic Rankine cycle (ORC), and other improved TCs. It was discovered that the efficiency of TC was always greater than that of ORC under the same conditions; however, water was not a suitable working fluid. Arbab et al. [19] compared the performance of ORC and TC power generation systems. The results showed that TC power generation system could utilize up to 70% of available power and had about 50% more power generation capability than ORC. Ajimotokan [20] conducted preliminary elections and intensive studies on the appropriate working fluid for the trilateral flash cycle and discovered that light hydrocarbons were more suitable as working fluids, and n-pentane was eventually chosen as the working fluid. The comparison of the thermodynamic performance of TC and three improved TCs was reported. The effects of expander inlet temperature and expander adiabatic efficiency on cycle performance were investigated. Antonopoulou et al. [21] simulated the trilateral flash cycle with Aspen Plus and compared the net output power, thermal efficiency, and exergy efficiency for different working fluids. The thermodynamic results showed that HFO-1234yf had the best power production and thermal efficiency at a heat source temperature of 90 °C, while HFC-245fa had a stronger exergy potential. Chang et al. [22] screened the working fluid from the perspective of the heat source and expander, finding that when the heat source temperature is close to the critical temperature of the working fluid, the system performance is better.

Moreover, geothermal energy thermodynamic cycles have been extensively reported in China [23,24]. Wang et al. [25] evaluated the thermo-economic performance of a dual-pressure ORC system powered by geothermal heat. A comparison of single and dual-pressure systems was performed. The effects of the annual loan interest rate, on-grid electricity price, and carbon tax on the system's economic performance were also discussed. Zhang et al. [26] studied the impacts of superheat and internal heat exchangers on the thermo-economic performance of ORCs based on fluid type and heat source.

As a bottom cycle, the TC is also able to recycle low-grade thermal energy from other scarce heat sources, including industrial waste heat or engine waste heat, in addition to recovering geothermal energy. Hays et al. [27] drove the TC system with waste heat from ship engines and conducted sea trials, confirming the reliability of TC applications for ships. Zeynali et al. [28] investigated the performance of modified trilateral flash cycles assisted by a solar pond and compared them with modified organic Rankine cycles. With the emergence of high-efficiency two-phase screw expanders, the application of TC has great development prospects.

In recent years, research of TC has made great progress, mainly in the selection of working fluid, application cases, the comparison between TC and traditional technology and the modeling and design of expander. However, the basic thermodynamic performance simulation and calculation methods, system optimization, and parameter analysis of TC are still rare. A deeper understanding of the fundamental thermodynamic performance of TC is required. Therefore, n-pentane is used as the working fluid and a twin-screw expander is chosen as the two-phase expander in the present work. Numerical simulations of the thermodynamic processes of TC are conducted. The influence of the system's main parameters on the cycle's thermodynamic performance is analyzed. The research is expected to make a significant addition to the study of TC's thermodynamic performance and provides guidance for the design and optimization of the TC waste heat recovery system.

2. Model Description and Conditions

2.1. System Specifications

Figure 1 shows the schematic diagram and temperature-enthalpy diagram of the TC system. The system is composed of a heater, a working fluid pump, a two-phase expander, and a condenser. The ideal TC includes four reversible processes: the isentropic compression process (1–2), constant pressure heating process (2–3), isentropic expansion process (3–4), and constant pressure exothermic process (4–1). In reality, the isentropic process is impossible to achieve in the pump and expander. The working fluid in the saturated liquid state (point 1) is compressed in the pump by the condensing pressure to the heating pressure and then delivered to the heater. Point 2 indicates the state of the working fluid at the heater inlet. In the heater, the working fluid is heated to the saturated liquid condition (point 3). Afterward, the working fluid is sent to the two-phase expander and go through the expansion process. At the same time, the working fluid's internal energy is turned into expander shaft power. The working fluid at the outlet of the expander (point 4) is in a gas-liquid two-phase state. The working fluid is then transported to the condenser, where the saturated vapor is converted to saturated liquid. Meanwhile, the latent heat of condensation of the working fluid is transferred to the condensing fluid. Finally, the working fluid returns to the saturated liquid condition (point 1). All the above processes constitute the whole cycle.

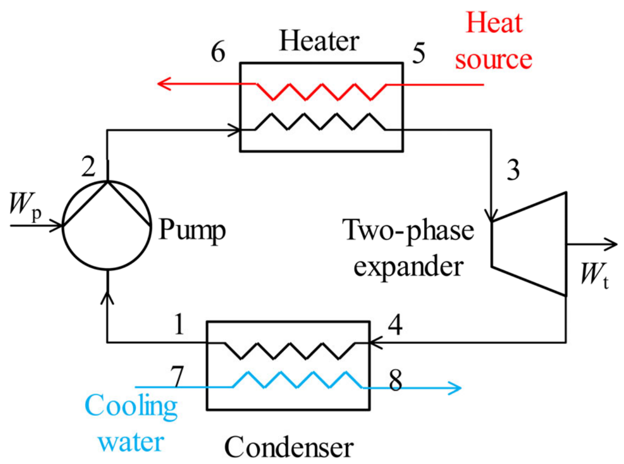

(**a**)

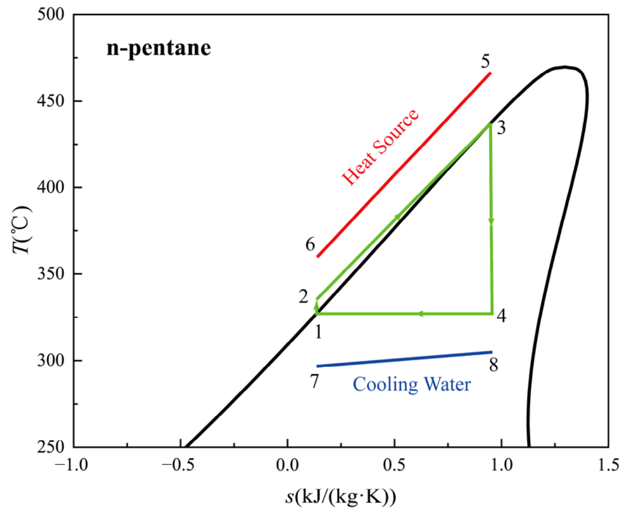

(**b**)

Figure 1. Schematic diagram (**a**) and temperature-enthalpy diagram (**b**) of the TC system.

2.2. Model Establishment

2.2.1. Thermodynamic Model of TC Internal Circulation

Some hypotheses are presented below to simplify the calculations. (1) The system is in the steady state. (2) The law of conservation of energy is followed by all system components. (3) Kinetic and potential energy changes of the working fluid are neglected. (4) Heat exchanger pressure drop and heat loss are not taken into account.

For the actual process, the compression process in the pump and the expansion process in the expander are both incomplete adiabatic processes, which cannot be precisely represented in the software. As a result, the adiabatic efficiency of the pump and expander are taken as empirical values. The detailed thermodynamic description of TC is summarized as follows:

Process 1–2: the power consumed by the pump:

$$w_{\text{pump}} = h_2 - h_1 = \frac{h_{2,s} - h_1}{\eta_{\text{pump}}} \tag{1}$$

where $h_{2,s}$ is the specific enthalpy after the process of the adiabatic compression of the working fluid. η_{pump} is the adiabatic efficiency of the pump.

Process 2–3: the heat absorbed from the heat source:

$$q_{\mathrm{h}} = h_3 - h_2 \tag{2}$$

Process 3–4: the power output of the expander:

$$w_{\mathrm{exp}} = h_3 - h_4 = \eta_{\mathrm{exp}} \cdot (h_3 - h_{4,\mathrm{s}}) \tag{3}$$

where $h_{4,\mathrm{s}}$ is the specific enthalpy of the working fluid after adiabatic expansion. η_{exp} is the adiabatic efficiency of the expander.

Process 4–1: the heat released by the working fluid in the condenser:

$$q_{\mathrm{c}} = h_4 - h_1 \tag{4}$$

The net power output of the system:

$$w_{\mathrm{net}} = w_{\mathrm{exp}} - w_{\mathrm{pump}} \tag{5}$$

The thermal efficiency of the system:

$$\eta_{\mathrm{th}} = w_{\mathrm{net}} / q_{\mathrm{h}} \tag{6}$$

The exergy of the working fluid at the state point i:

$$e_{x,i} = (h_i - h_0) - T_0(s_i - s_0) \tag{7}$$

where T_0 is the ambient temperature. h_0 and s_0 are the specific enthalpy and specific entropy of the working fluid at ambient temperature, respectively.

The heat exergy of the working fluid in the process 2–3:

$$e_{x,Q} = e_{x,3} - e_{x,2} \tag{8}$$

By substituting Equation (7) into Equation (8), the heat exergy of the working fluid can be expressed as follows:

$$e_{x,Q} = (h_3 - h_2) - T_0(s_3 - s_2) \tag{9}$$

The description of the exergy efficiency of TC is the following:

$$\eta_{\mathrm{ex}} = w_{\mathrm{net}} / e_{x,Q} \tag{10}$$

2.2.2. Heat Transfer Model of the Heater

The ε-NTU method [29] is adopted in the present work since the ε-NTU method can overcome the problem that multiple iterations should be conducted for the logarithmic mean temperature difference (LMTD) method [30]. Additionally, the ε-NTU method is commonly employed in the computation of low-temperature heat exchangers. The heat transfer model of the heater is established under the conditions of a given heat source, working fluid inlet temperature, and heat source fluid average heat-capacity flow rate.

To evaluate the performance of a heat exchanger, the parameter effectiveness of heat exchanger ε is utilized. It is defined as follows:

$$\varepsilon = \frac{|T_{\mathrm{out}} - T_{\mathrm{in}}|_{\mathrm{max}}}{T_5 - T_2} \tag{11}$$

where $|T_{\mathrm{out}} - T_{\mathrm{in}}|_{\mathrm{max}}$ is the maximum temperature difference between the inlet and outlet of the heat source fluid and the working fluid. T_5 is the inlet temperature of the heat source fluid. T_2 is the inlet temperature of the working fluid.

According to the energy balance:

$$Q_{\mathrm{h}} = C_{\mathrm{hc}}(T_5 - T_6) = C_{\mathrm{wf}}(T_3 - T_2) \tag{12}$$

where C_{hc} is the average heat-capacity flow rate of the heat source fluid. C_{wf} is the average heat-capacity flow rate of the working fluid.

The actual heat transfer in the heater:

$$Q_{\mathrm{h}} = C_{\mathrm{min}}\varepsilon(T_5 - T_2) \tag{13}$$

By substituting Equation (13) into Equation (12), the outlet temperatures of the heat source fluid and working fluid in the heater can be described as the following, respectively:

$$T_6 = T_5 - \frac{C_{\mathrm{min}}\varepsilon}{C_{\mathrm{hc}}}(T_5 - T_2) \tag{14}$$

$$T_3 = T_2 + \frac{C_{\mathrm{min}}\varepsilon}{C_{\mathrm{wf}}}(T_5 - T_2) \tag{15}$$

The effectiveness of the counter-flow heat exchanger:

$$\varepsilon = \frac{1 - \exp[(-\mathrm{NTU})(1 - R_{\mathrm{C}})]}{1 - R_{\mathrm{C}}\exp[(-\mathrm{NTU})(1 - R_{\mathrm{C}})]} \tag{16}$$

where NTU is the number of transfer units. R_{C} is the ratio of heat-capacity flow rate.

$$\mathrm{NTU} = \frac{(kA)_{\mathrm{h}}}{C_{\mathrm{min}}} \tag{17}$$

$$R_{\mathrm{C}} = C_{\mathrm{min}}/C_{\mathrm{max}} \tag{18}$$

where $(kA)_{\mathrm{h}}$ is the total heat transfer coefficient of the heater.

The average specific heat capacity of the working fluid during the heating process is defined as the following:

$$c_{p,\mathrm{wf}} = \frac{h_3 - h_2}{T_3 - T_2} \tag{19}$$

The mass flow rate of the working fluid:

$$m_{\mathrm{wf}} = C_{\mathrm{wf}}/c_{p,\mathrm{wf}} \tag{20}$$

2.2.3. Heat Transfer Model of the Condenser

Assuming that the cooling water inlet temperature T_7 is constant, the heat transfer in the condenser Q_{c} can be obtained from the heat balance equation [31]:

$$Q_{\mathrm{c}} = C_{\mathrm{ca}}(T_8 - T_7) = m_{\mathrm{wf}}(h_4 - h_1) \tag{21}$$

The outlet temperature of cooling water:

$$T_8 = T_1 - \Delta T_{\mathrm{P}} \tag{22}$$

where ΔT_{p} is the condenser pinch temperature difference.

The average heat-capacity flow rate of cooling water:

$$C_{ca} = \frac{m_{\mathrm{wf}}(h_4 - h_1)}{(T_8 - T_7)} \tag{23}$$

When the specific heat capacity of the cooling water $c_{p,\mathrm{ca}}$ is regarded as a constant, the mass flow rate of the cooling water m_{ca} is depicted as follows:

$$m_{ca} = C_{\mathrm{ca}} / c_{p,\mathrm{ca}} \tag{24}$$

The total heat transfer coefficient in the heater and condenser is described as follows:

$$kA_i = \dot{Q}_i / \Delta T_i \tag{25}$$

where ΔT_{i} is the logarithmic mean temperature difference of heat transfer. ΔT_{i} can be obtained in the following form:

$$\Delta T_i = \frac{\Delta T_{i,\max} - \Delta T_{i,\min}}{\ln(\Delta T_{i,\max} / \Delta T_{i,\min})} \tag{26}$$

The total heat transfer coefficient of the system:

$$(kA)_{\mathrm{tot}} = (kA)_{\mathrm{h}} + (kA)_{\mathrm{c}} \tag{27}$$

where $(kA)_{\mathrm{c}}$ is the total heat transfer coefficient of the condenser.

2.2.4. Model of the Second Law for the Thermodynamic Performance of the TC Heat Recovery and Power Conversion System

The heat exergy absorbed by the working fluid:

$$E_{x,Q,\mathrm{wf}} = m_{\mathrm{wf}}(e_{x3} - e_{x2}) \tag{28}$$

The heat exergy released by the heat source fluid:

$$E_{\mathrm{x},Q,\mathrm{hc}} = m_{\mathrm{hc}}(e_{x5} - e_{x6}) \tag{29}$$

The heat exergy released by the working fluid:

$$E_{x,c,\mathrm{wf}} = m_{\mathrm{wf}}(e_{x4} - e_{x1}) \tag{30}$$

The heat exergy absorbed by the cooling water:

$$E_{x,c,\mathrm{ca}} = m_{\mathrm{ca}}(e_{x8} - e_{x7}) \tag{31}$$

Among Equations (28)–(31), e_{x1}–e_{x8} indicate the exergy of per unit quality of working fluid, heat source fluid, or cooling water in each state point, respectively. $E_{x,\mathrm{Q,wf}}$ and $E_{x,\mathrm{c,wf}}$ represent the heat exergy absorbed by the working fluid during heating and released during condensation, respectively. $E_{x,\mathrm{Q,hc}}$ and $E_{x,\mathrm{c,ca}}$ represent the heat exergy released by the heat source fluid during the heating process and the heat exergy absorbed by the cooling water during the condensation process, respectively.

The exergy efficiency of the system:

$$\eta_{\mathrm{ex}} = \frac{W_{\mathrm{net}}}{E_{\mathrm{x},Q,\mathrm{hc}}} \tag{32}$$

The objective functions considered in the present paper are shown as follows.

For the TC internal circulation, the thermal efficiency of the system η_{th}, exergy efficiency η_{ex}, net power output W_{net} and heat absorption q_{h} are selected as the objective functions. To match the real conditions, the variation of the expansion ratio R_{exp} and the dryness at the outlet of the expander x_3 with the cycle parameters is calculated.

For the TC heat recovery and power conversion system, the performance of the system depends not only on the thermal efficiency of the cycle, but also greatly on the heat transfer efficiency of the heat source to the system. Furthermore, it is also related to the heat release of the system to the environment. Hence, the thermal efficiency η_{th}, exergy efficiency η_{ex}, net power output W_{net} and heat absorption q_h are considered as objective functions. Besides, taking the economic efficiency into consideration, the total heat transfer coefficient of the heater and condenser of the system, i.e., $(kA)_h$ and $(kA)_c$, is calculated.

2.3. Model Validation

Comparisons of thermodynamic performance between TC and ORC were made by Fischer et al. [17,18], who used the exergy efficiency as the objective function. The minimum heat-capacity flow rate of heat source fluid for 1MW net power output is obtained through the optimization calculation under five preset conditions. The theoretical model established in the previous section is verified under the same conditions as the first set of parameters.

Since water is the working fluid in Refs. [17,18], the adiabatic efficiency of the pump and the expander are set at 0.65 and 0.85, respectively. The net power output is 1 MW. The goal is to obtain the minimum heat-capacity flow rate of the heat source fluid via system optimization and determine the parameters at each state point of the cycle. In the present work, the thermal efficiency is calculated based on the parameters at each state point in Refs. [17,18].

Comparisons of the thermal efficiency between the results in the reference and the present work are listed in Table 1. It is shown that the thermal efficiency of the present model is less than that of Fischer's work. This is because the pump power consumption is considered in the present work while it is ignored in Fischer's work. Therefore, the pump power consumption is responsible for the difference.

Table 1. Validation of the model.

Parameters	T_1/K	T_2/K	T_3/K	T_4/K	p_1/kPa	p_3/kPa	η_{th}/%
Fischer's work	358.15	360.21	590	358.15	57.87	10,861	0.198
Present work	358.15	360.21	590	358.15	57.87	10,861	0.1947

2.4. Calculation Conditions

Since n-pentane is the working fluid, the critical pressure and temperature of n-pentane are 3.37 MPa and 469.5 K, respectively. According to the properties of the working fluid, the boundary parameters of the cycle are listed in Table 2.

Table 2. Boundary parameters of the TC.

Parameters	Value	Unit
Heat source fluid inlet temperature T_5	423	K
Pump adiabatic efficiency η_{pump}	85	%
Expander adiabatic efficiency η_{exp}	85	%
Ambient temperature T_0	298.15	K
Working fluid temperature range	309–496.5	K
Cooling water inlet temperature T_7	298.15	K
Condenser pinch temperature difference ΔT_p	5	K

3. Theoretical Analysis and Numerical Simulation Results of the TC Internal Circulation

3.1. Thermodynamic Performance of the TC Internal Cycle: A Theoretical Analysis

Under the condition of ignoring the power consumed by the pump, the thermal efficiency of the ideal TC is derived in Refs. [17,18] as the following form:

$$\eta_{th} = 1 - \frac{T_1 \cdot \ln(T_3 / T_1)}{T_3 - T_1} \tag{33}$$

In the present work, the pump power consumption is considered, and the derivation process is similar to that in Ref. [17]. Therefore, more details can be seen in Ref. [17]. Based on the established model, the thermal efficiency of the ideal TC that ignores the pump power consumption could be described as follows:

$$\eta_{\mathrm{th}} = 1 - \frac{T_1 \cdot \ln(T_3\,/\,T_2)}{T_3 - T_2} \tag{34}$$

The exergy efficiency of the ideal TC could be written as:

$$\eta_{\mathrm{ex}} = w_{\mathrm{net}}/e_{x,Q} = \frac{T_3 - T_2 - T_1 \cdot \ln(T_3/T_2)}{T_3 - T_2 - T_0 \cdot \ln(T_3/T_2)} \tag{35}$$

It is known that the thermal efficiency is only related to T_1, T_2, and T_3 in Equation (34). Since T_1 can be determined by the parameters at state point 2 and the adiabatic efficiency of the pump, the thermal efficiency is actually related to T_2 and T_3.

The first-order derivatives of η_{th} to T_2 and T_3 for Equation (34) are calculated, respectively. When $T_3 > T_2$, the following results can be obtained.

$$\frac{\mathrm{d}\eta_{\mathrm{th}}}{\mathrm{d}T_2} = \frac{T_1[1/T_2 - \ln(T_3/\,T_2)]}{(T_3 - T_2)^2} < 0 \tag{36}$$

$$\frac{\mathrm{d}\eta_{\mathrm{th}}}{\mathrm{d}T_3} = \frac{T_1[\ln(T_3/T_2) - (1 - T_2/T_3)]}{(T_3 - T_2)^2} > 0 \tag{37}$$

From Equations (36) and (37), it can be predicted that the η_{th} decreases with the increase of T_2 but increases with the increase of T_3.

Through similar conduction to Equation (35) with that to Equation (34), Equations (38) and (39) are obtained when $T_3 > T_2$, the following results can be obtained.

$$\frac{\mathrm{d}\eta_{\mathrm{ex}}}{\mathrm{d}T_2} < 0 \tag{38}$$

$$\frac{\mathrm{d}\eta_{\mathrm{ex}}}{\mathrm{d}T_3} > 0 \tag{39}$$

It is predicted that η_{ex} decreases with the increase of T_2 and increases with the increase of T_3.

3.2. Analysis of Numerical Simulation Results of the TC Internal Circulation

In this section, the heat absorption of the cycle Q_{h}, the net power output W_{net}, the thermal efficiency η_{th}, and the exergy efficiency η_{ex} are regarded as objective functions to determine the effect of T_2 and T_3 on the thermodynamic performance of the cycle by EES. What's more, the thermal efficiency and exergy efficiency by numerical simulation are compared with those by theoretical analysis.

3.2.1. Effect of the Heater Inlet Temperature on Thermodynamic Performance

Given that the expander inlet temperature T_3 is set at 150 °C and the expander inlet pressure P_3 is set at 1591 kPa (the saturation pressure at 150 °C), the variation trends of the thermodynamic performance are varied with the increase of the temperature T_2, as depicted in Figure 2. It is obvious that the heat absorption of the cycle and the power output of the expander show increasing trends, and the pump power consumption is reduced with the decrease of T_2 when the expander inlet temperature T_3 is constant, which means W_{net}, η_{th}, and η_{ex} are all increased with the decrease of T_2. However, the variation trend of T_1 behaves the opposite, and the corresponding saturation pressure (expander outlet pressure) drops. When P_1 = 101 kPa and T_1 = 35.78 °C, a smaller T_2 will result in a lower expander outlet pressure, which will increase the condenser power consumption for vacuuming. According to Figure 2b, η_{th} and η_{ex} by numerical simulations are lower than those by theoretical calculations. The reason is due to the irreversibility of the actual process and the change in specific heat capacity with temperature.

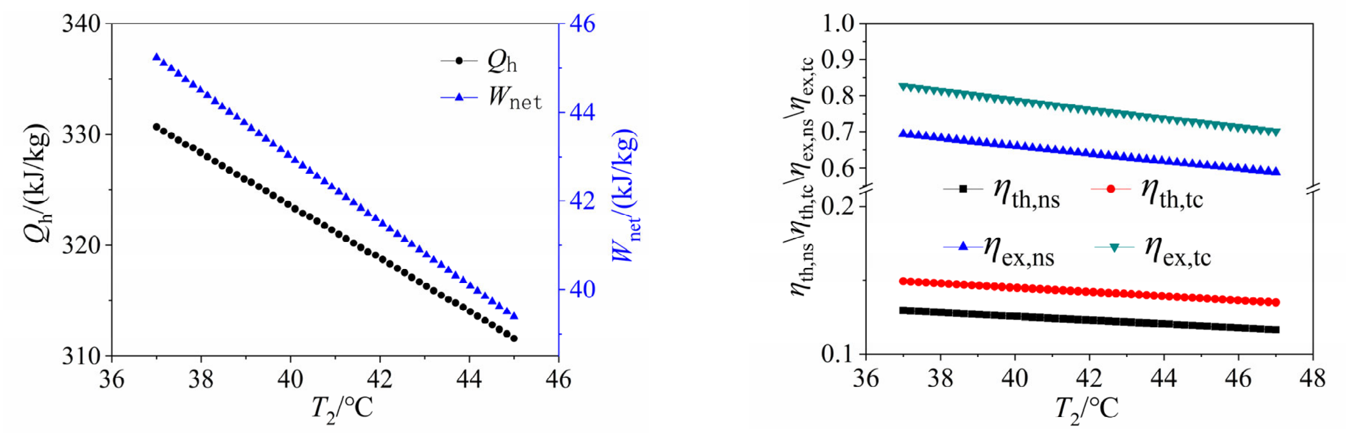

(**a**) (**b**)

Figure 2. The variation of thermodynamic performance with T_2: (**a**) Q_h and W_{net}; (**b**) the thermal efficiency and exergy efficiency by numerical simulations ($\eta_{th,ns}$ and $\eta_{ex,ns}$) and those by theoretical calculations ($\eta_{th,tc}$ and $\eta_{ex,tc}$).

3.2.2. Effect of the Expander Inlet Temperature on Thermodynamic Performance

In this section, the heater inlet temperature T_2 is held constant at 38 °C and T_3 is varied in the range of 125–195 °C. The variation trend of the objective functions with T_3 is displayed in Figure 3. The results show that as T_3 increased, as did Q_h, W_{net}, η_{th}, and η_{ex}. This is because the higher T_3 is, the higher the corresponding saturation pressure P_3 is, but the lower T_1 and P_1 are. Consequently, the power output of the expander and the power consumed by the pump are increased. η_{th} and η_{ex} ranged between 10–20% and 50–90%, respectively. η_{th} and η_{ex} obtained by numerical simulation were less than those obtained by theoretical calculation. More explanations can be found in the above section.

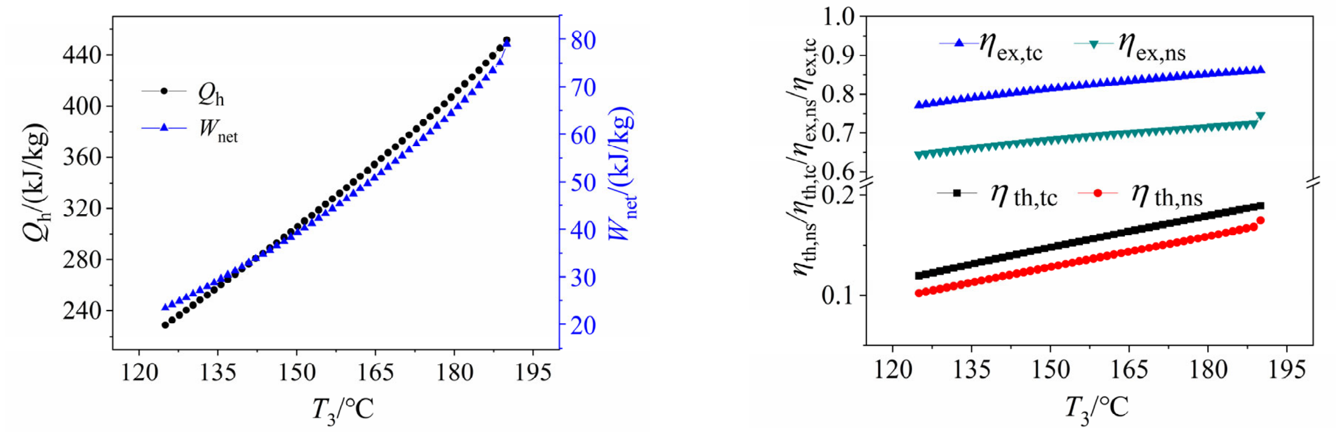

(**a**) (**b**)

Figure 3. The variation of thermodynamic performance with T_3: (**a**) Q_h and W_{net}; (**b**) the thermal efficiency and exergy efficiency by numerical simulations ($\eta_{th,ns}$ and $\eta_{ex,ns}$) and those by theoretical calculations ($\eta_{th,tc}$ and $\eta_{ex,tc}$).

3.2.3. Effect of the Heater Inlet Temperature and Expander Inlet Temperature on the Expansion Ratio and Dryness at the Outlet of the Expander

As shown in Figure 4a, when T_3 = 150 °C, the expansion ratio R_{exp} rose from 83.66 to 116.1 as T_2 reduced from 46 to 36.61 °C. As described in Figure 4b, when T_2 = 38 °C, R_{exp} rose from 92.59 to 117.4, with T_3 rising from 125 to 163.3 °C. As R_{exp} increased, the dryness at the expander outlet x_4 increased. Because the screw expander can expand with liquid, the dryness has slight damage to the expander. However, an excessive R_{exp} requires a large expander size, which leads to too much investment. As a result, the suitable R_{exp} should be determined by the actual production level before deciding the cycle parameters.

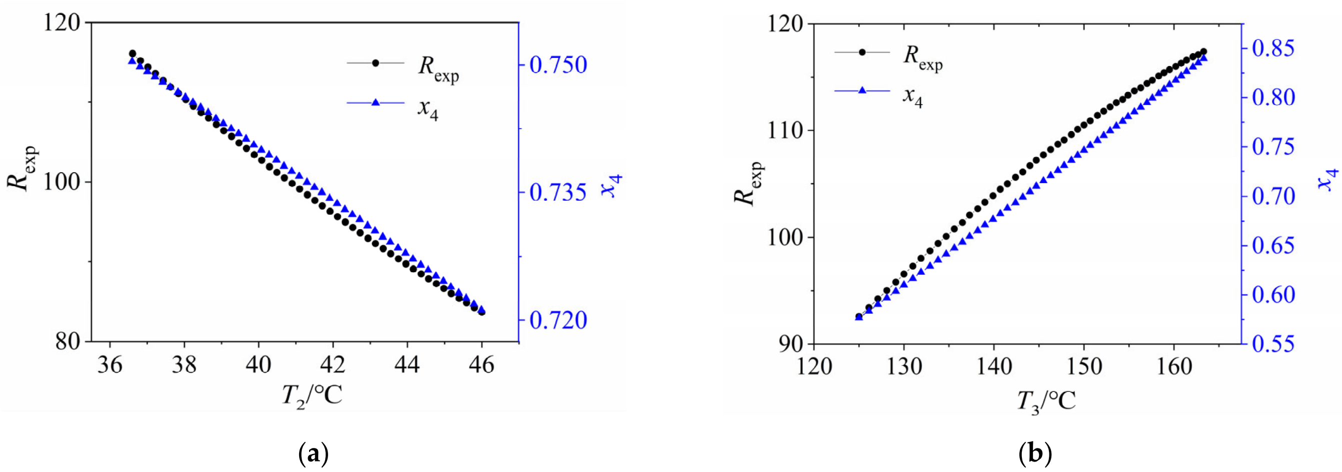

Figure 4. The variation of expansion ratio and dryness at the outlet of the expander with (**a**) T_2; (**b**) T_3.

4. Simulation Results and Analysis of the TC Heat Recovery and Power Conversion System

4.1. Effect of the Average Heat-Capacity Flow Rate of the Working Fluid on Thermodynamic Performance

As depicted in Figure 5, when the effectiveness of the heater ε was 0.95, T_2 was 313 K, and the average heat-capacity flow rate of the heat source fluid C_{hc} was 5 kW/K, the system performance varied with the variation of the average heat-capacity flow rate of the working fluid C_{wf}. Under the condition of $C_{wf} < C_{hc}$, the heat absorption, heat release, and the net power output of the system increase with the increase of C_{wf}. At the same time, η_{th} maintained invariableness, and η_{ex} increased. According to Equation (15), it is known that $C_{min} = C_{wf}$ at this time, so T_3 remained unchanged. The condensing temperature T_1 was also calculated as a constant value according to the condenser model. Thus (h_3-h_2) and (h_3-h_4) were constant and Q_h and W_{net} increased as C_{wf} (i.e., m_{wf}) increased. Therefore, η_{th} remained constant. C_{wf} increased the need to change the heat exchanger model, the NTU also increased, and the $(kA)_h$ also increased, when C_{wf} and C_{hc} were equal, the W_{net} reached the maximum and $(kA)_h$ also reached the maximum. When $C_{wf} > C_{hc}$, with the increase of C_{wf}, T_3 decreased, evaporation pressure P_3 decreased, T_1 increased, heat source fluid outlet temperature T_6 remained unchanged, circulating heat absorption was the maximum value and remained unchanged, circulating heat release increased, W_{net} decreased, η_{ex} decreased, NTU and $(kA)_h$ both decreased.

Under the condition of C_{wf} higher than C_{hc}, heat absorption of the cycle keeps constant and reaches its maximum even if C_{wf} increased. At the same time, the heat release of the cycle increased. Contrarily, W_{net}, η_{ex}, NTU, and $(kA)_h$ showed the opposite variety. When C_{wf} changes between 1 kW/K and 10 kW/K, the highest η_{th} and the lowest η_{th} of the cycle were 12.8 and 6.63%, respectively. By calculating the power output of the expander W_{exp} and the power consumed by the pump W_{pump}, it was found that with the increase of C_{wf}, the ratio of W_{pump} to W_{exp} rose from 0.07 to 0.08, which means the power consumed by the pump in the system cannot be ignored.

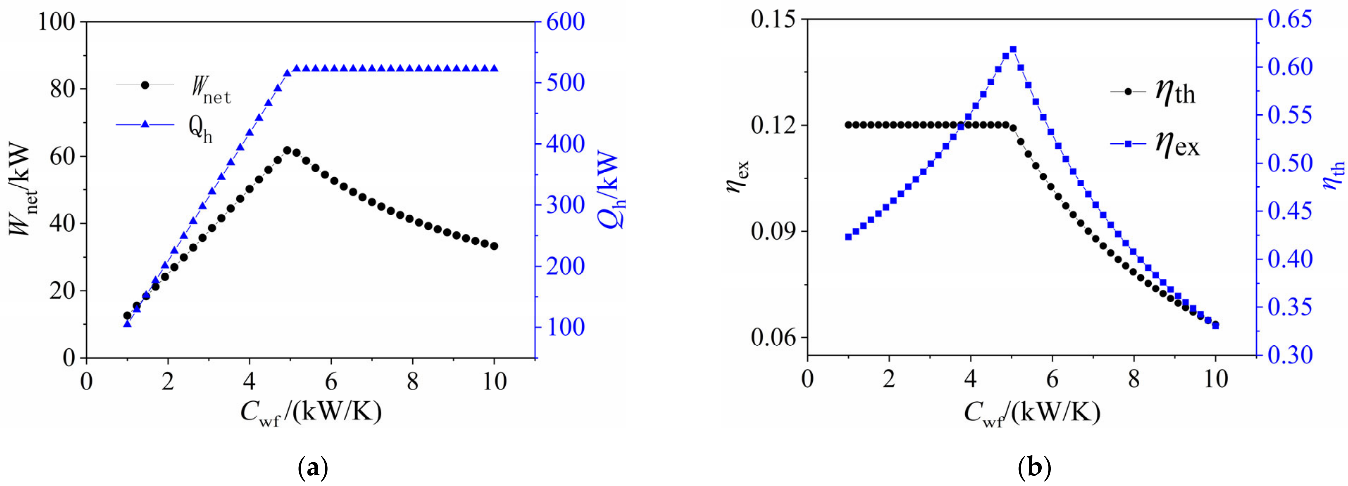

Figure 5. The impact of C_{wf} on the thermal performance of the system for a constant ε: (**a**) Q_h and W_{net}; (**b**) η_{th} and η_{ex}.

When the total heat transfer coefficient of the heater $(kA)_h$ was kept at 20 kW/K, the performance of the system was varied with C_{wf}, as shown in Figure 6. It was demonstrated that with the increase of C_{wf}, η_{th}, and η_{ex} decreased gradually. Meanwhile, Q_h increased gradually, and W_{net} increased first and then decreased. In other words, there was a maximum W_{net}. This is because, with the increase of C_{wf}, T_3 decreased while T_4 was basically unchanged, which led to a reduction in W_{exp} by unit working fluid. When the working fluid flow rate was within a suitable range, the increase in the flow rate of the working fluid can make up for the decrease of W_{exp}, which leads to a rise in the overall output power. The maximum net power output was obtained when the working fluid flow rate reachedthe critical value. Subsequently, the increase in the working fluid flow rate cannot compensate for the decrease in W_{exp} per unit mass of the working fluid. Consequently, W_{net} decreased. Similarly, W_{exp} first increased and then decreased with the increase of C_{wf}.

4.2. Effect of the Average Heat-Capacity Flow Rate of the Working Fluid on the Heat Transfer Capacity of the System

Figure 7a depicts the variation trends of the total heat transfer coefficient of the heater $(kA)_h$ and condenser $(kA)_c$, as well as the sum of the two coefficients $(kA)_{tot}$, with C_{wf} when $\varepsilon = 0.95$ and $C_{hc} = 5$ kW/K. It reveals that $(kA)_h$ increased quickly and then decreased rapidly with the increase of C_{wf}. When $C_{wf} = C_{hc}$, $(kA)_h$ reached the highest value. The increased rate of $(kA)_c$ for $C_{wf} < C_{hc}$ was larger than that for $C_{wf} > C_{hc}$. Moreover, the conversion trend of $(kA)_{tot}$ showed great similarities to that of $(kA)_h$. As depicted in Figure 7a, when C_{wf} was close to C_{hc}, $(kA)_h$ was greater than $(kA)_c$. In other cases, $(kA)_c$ was bigger than $(kA)_h$. According to the simulation results in Section 4.2, when $C_{wf} = C_{hc}$, W_{net} attained its maximum value. At the same time, $(kA)_h$ reached the maximum of 88.3 kW/K. Taking the investment of the heat exchanger into account, the system economy is not necessarily good when W_{net} is at its maximum.

As shown in Figure 7b, at $(kA)_h = 20$ kW/K, $(kA)_c$ gradually increased and exceeded $(kA)_h$. However, the increased rate of $(kA)_c$ decreased gradually. Furthermore, $(kA)_{tot}$ increased with $(kA)_c$. As the simulation results mentioned above, W_{net} had a maximum value when $(kA)_h = 20$ kW/K and $C_{wf} = C_{hc}$. Nevertheless, the heater efficiency was minimum. Therefore, C_{wf} should be selected, reasonably based on the actual situation.

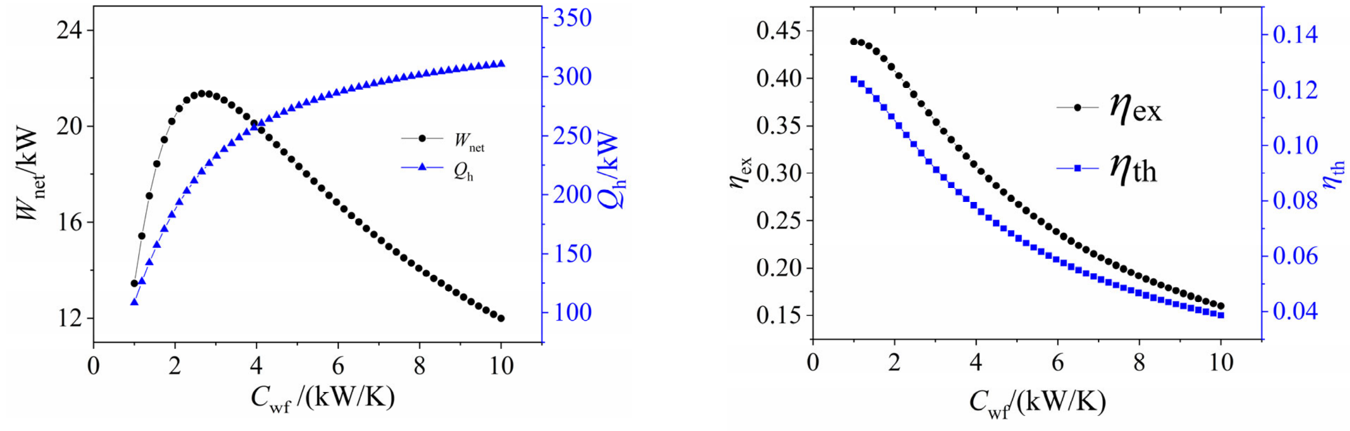

(**a**) (**b**)

Figure 6. The impact of C_{wf} on the thermal performance of the system for a constant $(kA)_h$: (**a**) Q_h and W_{net}; (**b**) η_{th} and η_{ex}.

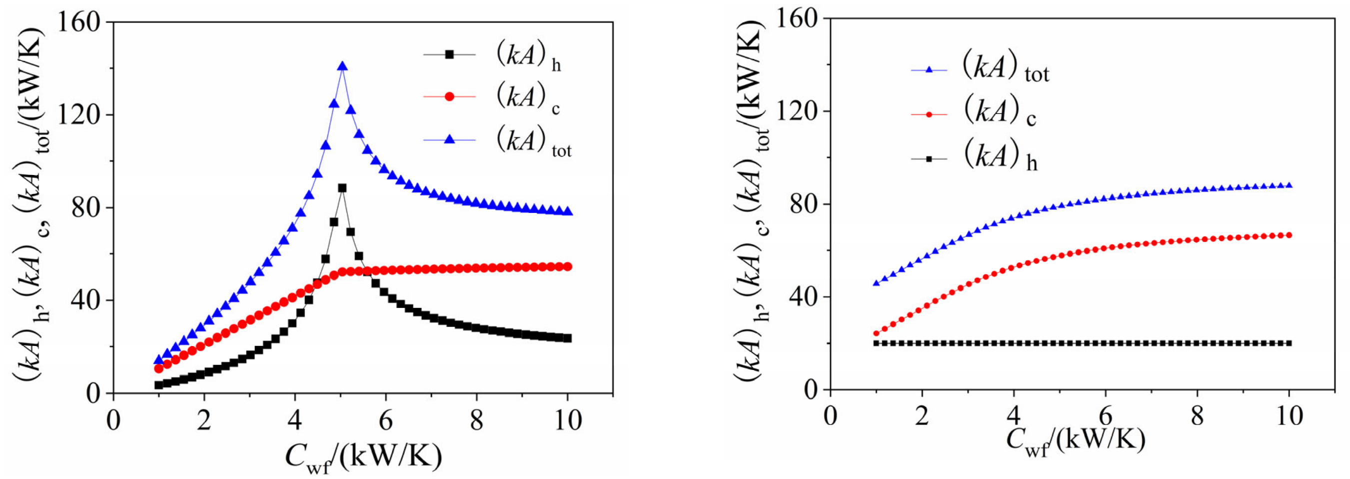

(**a**) (**b**)

Figure 7. The impact of C_{wf} on the heat transfer capacity of the system: (**a**) ε remains constant; (**b**) $(kA)_h$ remains constant.

5. Conclusions

This work developed a system model for a stable-flowing triangular cycle, simulated its thermodynamic process, and investigated the effects of key operational parameters on system performance. The following are the main conclusions:

(1) For the TC internal cycle, increasing T_3 and decreasing T_2 can improve the thermal efficiency and net power output of the cycle.

(2) For the TC heat recovery and power conversion system with constant parameters of the heat source fluid, the net power output increases at first and then decreases when ε or $(kA)_h$ is constant. The net power output can reach its maximum value at a certain average heat-capacity flow rate of the working fluid. In addition, the thermal efficiency and exergy efficiency should be taken into consideration as well; thus, a suitable objective function will be selected to optimize the thermodynamic performance of the system.

(3) For the TC heat recovery and power conversion system with constant parameters of the heat source fluid, when the total heat transfer coefficient of the heater $(kA)_h$ is constant, the heat transfer coefficient of the condenser $(kA)_c$ increases gradually with the increase of the average heat-capacity flow rate of the working fluid C_{wf}. Furthermore, $(kA)_c$ will

increase to a value that is greater than $(kA)_h$ for a relatively small $(kA)_h$. Under the condition that the effectiveness of the heater ε is 0.95, $(kA)_h$ increases first and then decreases. $(kA)_h$ will reach its maximum when $C_{wf} = C_{hc}$. $(kA)_c$ increases gradually, however, the increase rate decreases gradually for $C_{wf} > C_{hc}$.

(4) The performance of the TC will be improved when the heat transfer capacity between the working fluid and the heat source fluid and cooling water is enhanced. Besides, the balance of the investment and the performance of the system plays a significant role in reducing the cost of the heat exchanger and the wide application of TC. In the actual process, not only the heat transfer but also the increase in the amount of working fluid, heat source fluid, and cooling water significantly impact the net power output and thermal efficiency.

Author Contributions: Writing—original draft and methodology, L.L.; writing—review and editing and visualization, S.Z.; investigation, Y.J.; data curation, X.L.; validation, G.L.; resources, C.L.; data curation, Q.L.; software, H.G.; supervision and project administration, C.H. All authors have read and agreed to the published version of the manuscript.

Funding: This research was funded by the Science and Technology Innovation Talents in Universities of Henan Province (No.22HASTIT024).

Data Availability Statement: The data that support the findings of this study are available from the corresponding author upon reasonable request.

Conflicts of Interest: The authors declare that they have no known competing financial interests or personal relationships that could have appeared to influence the work reported in this paper.

Nomenclature

c_p	specific heat at constant pressure (kJ/kg)	c	condenser
C	the average heat-capacity flow rate (kW/K)	ca	cooling water
e	specific exergy (kJ/kg)	ex	exergy
E	exergy (kW)	exp	expansion
h	specific enthalpy (kJ/kg)	h	heater
(kA)	the heat transfer coefficient (kW/K)	hc	heat source fluid
m	mass flow rate (kg/s)	i	a state point
p	pressure (MPa)	in	inlet
q	specific heat absorption or heat release (kJ/kg)	max	maximum
Q	heat absorption or heat release (kW)	min	minimum
R	the ratio of average heat-capacity flow rate	net	net
s	specific entropy (kJ/(kg·K))	out	outlet
T	temperature (K)	pump	pump
ΔT	the pinch temperature difference (K)	s	ideal state point
w	specific power (kJ/kg)	th	thermal
W	power output or input (kW)	tot	total
x	dryness	wf	working fluid
Subscripts		*Greek symbols*	
0	environmental conditions	ε	effectiveness of heat exchanger
1–8	state points	η	efficiency

References

1. Javadi, M.A.; Ghomashi, H.; Taherinezhad, M.; Nazarahari, M.; Ghasemiasl, R. Comparison of Monte Carlo Simulation and Genetic Algorithm in Optimal Wind Farm Layout Design in Manjil Site Based on Jensen Model. In Proceedings of the 7th Iran Wind Energy Conference (IWEC2021), Shahrood, Iran, 17–18 May 2021. [CrossRef]
2. Chen, J.; Zhang, Y.; Xu, Z.; Li, C. Flow characteristics analysis and power comparison for two novel types of vertically staggered wind farms. *Energy* **2023**, *263*, 126141. [CrossRef]
3. Ancona, M.A.; Bianchi, M.; Branchini, L.; De Pascale, A.; Melino, F.; Peretto, A.; Poletto, C.; Torricelli, N. Solar driven micro-ORC system assessment for residential application. *Renew. Energy* **2022**, *195*, 167–181. [CrossRef]
4. Yang, J.; Li, J.; Yang, Z.; Duan, Y. Thermodynamic analysis and optimization of a solar organic Rankine cycle operating with stable output. *Energy Convers. Manag.* **2019**, *187*, 459–471. [CrossRef]

5. Bina, S.M.; Jalilinasrabady, S.; Fujii, H. Energy, economic and environmental (3E) aspects of internal heat exchanger for ORC geothermal power plants. *Energy* **2017**, *140*, 1096–1106. [CrossRef]
6. Surindra, M.D.; Caesarendra, W.; Prasetyo, T.; Mahlia, T.M.I.; Taufik. Comparison of the Utilization of 110 °C and 120 °C Heat Sources in a Geothermal Energy System Using Organic Rankine Cycle (ORC) with R245fa, R123, and Mixed-Ratio Fluids as Working Fluids. *Processes* **2019**, *7*, 113. [CrossRef]
7. Vélez, F.; Segovia, J.J.; Martín, M.C.; Antolín, G.; Chejne, F.; Quijano, A. A technical, economical and market review of organic Rankine cycles for the conversion of low-grade heat for power generation. *Renew. Sustain. Energy Rev.* **2012**, *16*, 4175–4189. [CrossRef]
8. Chan, C.; Ling-Chin, J.; Roskilly, A.P. A review of chemical heat pumps, thermodynamic cycles and thermal energy storage technologies for low grade heat utilisation. *Appl. Therm. Eng.* **2013**, *50*, 1257–1273. [CrossRef]
9. Hays, L.; Welch, P.; Boyle, P. The organic triangle cycle experience and status. *Energy Procedia* **2017**, *129*, 1034–1040. [CrossRef]
10. Iqbal, A.; Rana, S.; Ahmadi, M.; Date, A.; Akbarzadeh, A. Experimental study on the prospect of low-temperature heat to power generation using Trilateral Flash Cycle (TFC). *Appl. Therm. Eng.* **2020**, *172*, 115139. [CrossRef]
11. Iqbal, A.; Rana, S.; Ahmadi, M.; Date, A.; Akbarzadeh, A. Trilateral Flash Cycle (TFC): A promising thermodynamic cycle for low grade heat to power generation. *Energy Procedia* **2019**, *160*, 208–214. [CrossRef]
12. Smith, I.K. Development of the Trilateral Flash Cycle System: Part 1: Fundamental Considerations. *Proc. Inst. Mech. Eng. Part A J. Power Energy* **1993**, *207*, 179–194. [CrossRef]
13. Smith, I.K.; Da Silva, R.P.M. Development of the Trilateral Flash Cycle System Part 2: Increasing Power Output with Working Fluid Mixtures. *Proc. Inst. Mech. Eng. Part A J. Power Energy* **1994**, *208*, 135–144. [CrossRef]
14. Smith, I.K.; Stosic, N.; A Aldis, C. Development of the Trilateral Flash Cycle System: Part 3: The Design of High-Efficiency Two-Phase Screw Expanders. *Proc. Inst. Mech. Eng. Part A J. Power Energy* **1996**, *210*, 75–93. [CrossRef]
15. Bryson, M. *Conversion of Low Grade Heat into Electricity Using the Thermosyphon Rankine Engine and Trilateral Flash Cycle*; RMIT University: Melbourne, VIC, Australia, 2007.
16. Steffen, M.; Löffler, M.; Schaber, K. Efficiency of a new Triangle Cycle with flash evaporation in a piston engine. *Energy* **2013**, *57*, 295–307. [CrossRef]
17. Fischer, J. Comparison of trilateral cycles and organic Rankine cycles. *Energy* **2011**, *36*, 6208–6219. [CrossRef]
18. Lai, N.A.; Fischer, J. Efficiencies of power flash cycles. *Energy* **2012**, *44*, 1017–1027. [CrossRef]
19. Arbab, I.; Sohel, R.; Mahdi, A.; Thomas, C.; Abhijit, D.; Aliakbar, A. Prospects of Trilateral Flash Cycle (TFC) for Power Generation from Low Grade Heat Sources. *EDP Sci.* **2018**, *64*, 06004. [CrossRef]
20. Ajimotokan, H.A. *A Study of Trilateral Flash Cycles for Low-Grade Waste Heat Recovery-to-Power Generation*; Cranfield University: Cranfield, UK, 2014.
21. Antonopoulou, C.; Atsonios, K.; Grammelis, P.; Manolakos, D.; Skiadopoulos, A.; Bakalis, P. Thermodynamic Analysis on Trilateral Flash Cycle (TFC) for Low Grade Heat to Power Generation Using Different Working Fluids. In Proceedings of the 6th International Seminar on ORC Power Systems, online, 11–13 October 2021.
22. Chang, N.; Zhu, J.; Chen, G.; Zhang, P.; Song, A. Working fluids selection from perspectives of heat source and expander for a Trilateral cycle. *Energy Procedia* **2019**, *158*, 1579–1584. [CrossRef]
23. Feng, Y.; Chen, X.; Xu, X.F. Current status and potentials of enhanced geothermal system in China: A review. *Renew. Sustain. Energy Rev.* **2014**, *33*, 214–223. [CrossRef]
24. Zhang, D.; Wang, J.; Lin, Y.; Si, Y.; Huang, C.; Yang, J.; Huang, B.; Li, W. Present situation and future prospect of renewable energy in China. *Renew. Sustain. Energy Rev.* **2017**, *76*, 865–871. [CrossRef]
25. Wang, S.; Liu, C.; Zhang, C.; Xu, X.; Li, Q. Thermo-economic evaluations of dual pressure organic Rankine cycle (DPORC) driven by geothermal heat source. *J. Renew. Sustain. Energy* **2018**, *10*, 063901. [CrossRef]
26. Zhang, C.; Liu, C.; Xu, X.; Li, Q.; Wang, S.; Chen, X. Effects of superheat and internal heat exchanger on thermo-economic performance of organic Rankine cycle based on fluid type and heat sources. *Energy* **2018**, *159*, 482–495. [CrossRef]
27. Hays, L.; Otsuka, A.; Boyle, P. Sea Trials of an Organic Triangle System (OTC) for Waste Heat Recovery. In Proceedings of the 6th International Seminar on ORC Power Systems, Online, 11–13 October 2021.
28. Zeynali, A.; Akbari, A.; Khalilian, M. Investigation of the performance of modified organic Rankine cycles (ORCs) and modified trilateral flash cycles (TFCs) assisted by a solar pond. *Sol. Energy* **2019**, *182*, 361–381. [CrossRef]
29. Sphaier, L.; Worek, W. Parametric analysis of heat and mass transfer regenerators using a generalized effectiveness-NTU method. *Int. J. Heat Mass Transf.* **2009**, *52*, 2265–2272. [CrossRef]
30. Zhou, Y.; Tang, J.; Zhang, C.; Li, Q. Thermodynamic Analysis of the Air-Cooled Transcritical Rankine Cycle Using CO2/R161 Mixture Based on Natural Draft Dry Cooling Towers. *Energies* **2019**, *12*, 3342. [CrossRef]
31. Cengel, Y.A.; Klein, S.; Beckman, W. Heat Transfer: A Practical Approach. McGraw-Hill: Boston, MA, USA, 1998.